Title:

VMHdm/c^{SF-1} Neuronal Circuits Regulate Skeletal Muscle PGC1-α via the Sympathoadrenal Drive

Author:

Takuya Yoshida[1,2*], Scotlynn Farmer[1], Ami Harada[1,3], Zhen Shi[1,4], Jenny J. Lee[5], Arely Tinajero[5], Ashish K. Singha[1], Teppei Fujikawa[1,5#]

Affiliation:

1. Department of Cellular and Integrative Physiology, Long School of Medicine, University of Texas Health San Antonio, San Antonio, US

2. Department of Clinical Nutrition School of Food and Nutritional Sciences, University of Shizuoka, Shizuoka, Japan

3. Nara Medical University, Nara, Japan

4. Department of Plastic Surgery, Hospital Zhejiang University School of Medicine, Zhejiang, China

5. Center for Hypothalamic Research, Department of Internal Medicine, UT Southwestern Medical Center, Dallas, US

*Current Address: Laboratory of Clinical Nutrition, Division of Food and Health Environmental Sciences, Prefectural University of Kumamoto, Kumamoto, Japan

Corresponding Author: Teppei Fujikawa email: teppei.fujikawa@utsouthwestern.edu

Abstract

To adapt to metabolically challenging environments, the central nervous system (CNS) orchestrates metabolism of peripheral organs including skeletal muscle. The organ-communication between the CNS and skeletal muscle has been investigated, yet our understanding of the neuronal pathway from the CNS to skeletal muscle is still limited. Neurons in the dorsomedial and central parts of the ventromedial hypothalamic nucleus (VMHdm/c) expressing steroidogenic factor-1 (VMHdm/c^{SF-1} neurons) are key for metabolic adaptations to exercise, including increased basal metabolic rate and skeletal muscle mass in mice. However, the mechanisms by which VMHdm/c^{SF-1} neurons regulate skeletal muscle function remain unclear. Here, we show that VMHdm/c^{SF-1} neurons increase the sympathoadrenal activity and regulate skeletal muscle peroxisome proliferator-activated receptor gamma coactivator 1 alpha (PGC-1α) in mice via multiple downstream nodes. Optogenetic activation of VMHdm/c^{SF-1} neurons dramatically elevates mRNA levels of skeletal muscle *Pgc-1α*, which regulates a spectrum of skeletal muscle function including protein synthesis and metabolism. Mechanistically, the sympathoadrenal drive coupled with β2 adrenergic receptor (β2AdR) is essential for VMHdm/c^{SF-1} neurons-mediated increases in skeletal muscle PGC1-α. Specifically, adrenalectomy and knockout of β2AdR block augmented skeletal muscle PGC1-α by VMHdm/c^{SF-1} neuronal activation. Optogenetic functional mapping reveals that downstream nodes of VMHdm/c^{SF-1} neurons are functionally redundant to increase circulating epinephrine and skeletal muscle PGC1-α. Collectively, we propose that VMHdm/c^{SF-1} neurons-skeletal muscle pathway, VMHdm/c^{SF-1} neurons→multiple downstream nodes→the adrenal gland→skeletal muscle β2AdR, underlies augmented skeletal muscle function for metabolic adaptations.

Introduction

The central nervous system (CNS) orchestrates the whole-body metabolism[1,2]. Within the CNS, the hypothalamus plays a dominant role in the regulation of metabolic homeostasis in response to dynamic challenges such as hypoglycemia[3], cold-exposure[4], and exercise[5]. Our previous work articulates that neurons in the dorsomedial and central parts of ventromedial hypothalamic nucleus (VMHdm/c neurons) substantially contribute to metabolic adaptations to exercise training including augmented skeletal muscle mass and basal metabolic rate in mice[6]. Knockdown of steroidogenic factor-1 (SF-1)[7,8] in VMHdm/c neurons hampers exercise-induced mRNA expression of *peroxisome proliferator-activated receptor gamma coactivator 1 alpha* (*Pgc-1α*) in skeletal muscle[6]. PGC-1α is a key transcriptional regulator that controls a broad range of genes related to glucose and fat metabolism, mitochondrial function, angiogenesis, and protein synthesis[9,10]. Loss- or gain-of-function of PGC-1α in skeletal muscle dramatically changes skeletal muscle physiology as well as whole-body metabolism[11,12]. These data suggest that VMHdm/c neurons expressing SF-1 (VMHdm/c^{SF-1} neurons) mediate metabolic responses of skeletal muscle to exercise, thereby contributing to metabolic benefits of exercise. However, the mechanisms by which VMHdm/c^{SF-1} neurons mediate exercise-induced augmented skeletal muscle PGC-1α expression remains unclear. In particular, the pathway from VMHdm/c^{SF-1} neurons to skeletal muscle has yet to be unraveled.

PGC-1α expression in skeletal muscle is augmented by a variety of physiological stimuli[9,13]. For example, *ex vivo* muscle contraction is sufficient to increase mRNA levels of *Pgc-1α* by activation of calcium signaling pathways[14,15]. Notably, the adrenergic activation such as epinephrine, norepinephrine, and β-2 adrenergic receptors (β2AdR) agonist can dramatically increase mRNA levels of *Pgc-1α* in skeletal muscle[16,17]. In contrast, blocking the adrenergic

signaling by a systematic injection of β2AdR antagonist significantly hampers exercise-induced *Pgc-1α* mRNA in skeletal muscle[18]. Numerous studies have indicated that VMH neurons affect the sympathetic nervous system (SNS) activity[19,20]. Knockdown of SF-1 in VMHdm/c neurons suppresses exercise-induced epinephrine release[6]. These data indicate that VMHdm/c^{SF-1} neurons regulate skeletal muscle PGC-1α via the SNS. However, the functional neurocircuits underlying VMHdm/c^{SF-1} neuronal regulation of the SNS are still unclear. A genetic labeling study using *Sf-1*-Cre mice, which express Cre-recombinase in VMHdm/c in adults, portraits that VMHdm/c neurons highly innervate to several areas that regulate the SNS activity, including the anterior bed nucleus of the stria terminalis (aBNST), preoptic area (POA), anterior hypothalamus area (AH), paraventricular hypothalamic nucleus (PVH), and periaqueductal gray (PAG)[21]. Although studies using optogenetics have identified that distinct downstream sites of VMHdm/c^{SF-1} neurons regulate blood glucose[22], defensive behaviors[23], and food intake[24], the vital downstream node of VMHdm/c^{SF-1} neurons regulating the SNS is unknown.

In this study, we used optogenetics and genetically-engineered mice to determine the key downstream nodes of VMHdm/c^{SF-1} neurons that regulate skeletal muscle PGC-1α via the SNS. We found that epinephrine release by the sympathoadrenal activity coupled with β2AdR is essential for VMHdm/c^{SF-1} neuronal-induced skeletal muscle PGC-1α. Furthermore, our results demonstrated that VMHdm/c^{SF-1} neurons regulate the SNS through functionally redundant circuits with the PVH and PAG acting as the main downstream nodes.

Results

Optogenetic VMHdm/c^{SF-1} neuronal activation induces skeletal muscle *Pgc-1α* mRNA expression

To determine the neuronal mechanism by which VMHdm/c^{SF-1} neurons regulate skeletal muscle function via the SNS, we generated mice expressing channelrhodopsin 2(H134R)[25](ChR2) specifically in VMHdm/c^{SF-1} neurons by microinjection of adeno-associated virus (AAV) bearing Cre-dependent ChR2 fused with fluorescent reporters (AAV-DIO-ChR2) into *Sf-1* Cre mice[26] (VMHdm/c^{SF-1}::ChR2, Figure 1A). We used AAV containing Cre-dependent mCherry for control (VMHdm/c^{SF-1}::mCherry). We used the following stimulation configurations; 5 ms duration, 20 Hz, 2 seconds activation/2 seconds resting cycle for 30 minutes (Figure 1B). We confirmed that our optogenetic configuration significantly induced Fos protein expression, a neuronal activation marker, in the stimulated side of the VMHdm/c, but not in the non-stimulated side (Figure 1C). Similar to previous studies[22,27,28], VMHdm/c^{SF-1} neuronal activation increased blood glucose (Figure 1D). In addition, we observed that VMHdm/c^{SF-1} neuronal activation induced increases in plasma glucagon without changing plasma insulin levels (Figure 1E and F). Next, we determined whether VMHdm/c^{SF-1} neuronal activation can induce transcriptional changes in skeletal muscle. PGC-1α is a key transcriptional regulator for a spectrum of genes governing glucose and fat metabolism, oxidative capacity, protein synthesis and degradation, and vascularization[9,10,13]. Importantly, *Pgc-1α* mRNA induction can be used as a readout of exercise-related skeletal muscle transcriptional changes because a single exercise training dramatically increases mRNA levels of *Pgc-1α*[6,13]. PGC-1α has several isoforms such as PGC1a-1, -2, -3 and -4[29]. We found that 30 minutes of VMHdm/c^{SF-1} neuronal activation is sufficient to induce *Pgc-1α-2, -3,* and *-4* mRNA

levels in tibialis anterior (TA) skeletal muscle (Figure 1G). We then measured plasma catecholamines levels after VMHdm/c^{SF-1} neuronal activation. Interestingly, plasma epinephrine levels were significantly increased by VMHdm/c^{SF-1} neuronal activation, but norepinephrine levels in VMHdm/c^{SF-1} neuronal activated mice were not significantly different from control group (Figure 1 H and I). Previous studies have shown that optogenetic VMHdm/c^{SF-1} neuronal activation elicits behavioral changes such as freeze and burst activity (combination of freeze, jump, and run)[23,30]. In line with that, we found that VMHdm/c^{SF-1} neuronal activation induced freeze or burst activity (17 cases of freeze (55%), 14 cases of burst activity (45%); total 31 trials). However, we did not observe any differences of skeletal muscle *Pgc-1α* mRNA levels between mice showed freeze and burst activity (SFigure 1), suggesting that the burst activity is unlikely to contribute to VMHdm/c^{SF-1} neurons-induced *Pgc-1α* expression. Collectively, these data indicate that VMHdm/c^{SF-1} neurons regulate skeletal muscle function via sympathoadrenal activity, as the adrenal gland is the only organ able to secret epinephrine into circulation.

The adrenal gland is essential for VMHdm/c^{SF-1} neuronal regulation of skeletal muscle

Next, to determine whether epinephrine release from the adrenal gland is required for VMHdm/c^{SF-1} neurons-induced skeletal muscle *Pgc-1α*, we surgically removed the adrenal gland, and then stimulated VMHdm/c^{SF-1} neurons. Sham surgery were used as surgical controls. As we expected, the adrenalectomy (ADX) eliminated blood corticosterone (Figure 2B). ADX mice were supplied with corticosterone in the drinking water to maintain the physiological levels of blood corticosterone (Figure 2C). We carried out optogenetic stimulation five days after ADX. ADX appeared not to affect Fos induction in the VMH (Figure 2D), suggesting ADX does not affect the ability of VMHdm/c^{SF-1} neuronal activation. Indeed, plasma glucagon levels were significantly

134 higher in ADX mice after VMHdm/c^{SF-1} neuronal activation (Figure 2E). Stunningly, ADX
135 completely blocked the effects of VMHdm/c^{SF-1} neuronal activation on blood glucose (Figure 2F),
136 and skeletal muscle *Pgc-1α* expression (Figure 2G), suggesting that the sympathoadrenal drive,
137 specifically the epinephrine release, is essential for VMHdm/c^{SF-1} neuronal regulation of skeletal
138 muscle function. In addition, these data suggest that glucagon release unlikely contributes to
139 VMHdm/c^{SF-1} neuronal-induced blood glucose levels.
140

141 **β2AdR is required for VMHdm/c^{SF-1} neuronal-induced skeletal muscle *Pgc-1α***

142 We assessed the contribution of β2AdR in VMHdm/c^{SF-1} neuronal-induced skeletal
143 muscle *Pgc-1α* expression. β2AdR is the major form of adrenergic receptors in skeletal muscle[31].
144 β2AdR agonist injection increases skeletal muscle *Pgc-1α-2, -3,* and *-4* mRNA levels[16], suggesting
145 that the sympathetic input coupled with β2AdR is key for skeletal muscle physiology. We tested
146 whether β2AdR global knockout (KO) can diminish VMHdm/c^{SF-1} neuronal-induced skeletal
147 muscle *Pgc-1α* expression (Figure 3A). We first determined whether β2AdR KO affects the ability
148 of ChR2 to activate VMHdm/c^{SF-1} neurons. Optogenetic stimulation induced equal levels of Fos
149 expression in the VMH of wild-type and β2AdR KO mice (VMHdm/c^{SF-1}::ChR2-WT and
150 VMHdm/c^{SF-1}::ChR2-β2AdR^{KO}, Figure 3B), suggesting β2AdR KO does not affect the capacity
151 for optogenetic activation of VMHdm/c^{SF-1} neurons. Blood glucose and plasma glucagon in
152 VMHdm/c^{SF-1}::ChR2-β2AdR^{KO} were significantly higher than that of control group (VMHdm/c^{SF-}
153 ^{1}::mCherry-β2AdR^{KO}) (Figure 3C and D). In addition, optogenetic stimulation of VMHdm/c^{SF-1}
154 neurons significantly increased plasma epinephrine in β2AdR KO compared to non-stimulation
155 control (Figure 3E). VMHdm/c^{SF-1}::ChR2-β2AdR^{KO} showed significantly lower mRNA levels of
156 skeletal muscle *Pgc-1α-2, -3,* and *-4* compared to VMHdm/c^{SF-1}::ChR2-WT (Figure 3F).

157 Collectively, these results demonstrate that β2AdR is essential for VMHdm/c^{SF-1} neuronal-induced
158 skeletal muscle transcriptional regulation, but not blood glucose levels.
159
160 **Redundant functionality of downstream nodes of VMHdm/c^{SF-1} neurons**
161 VMHdm/c^{SF-1} neurons project to a broad range of the CNS sites that regulate the SNS
162 including presympathetic nodes[21]. Among these areas, we examined the contributions of the
163 aBNST, POA, AH, PVH/AH, and PAG to VMHdm/c^{SF-1} neuronal-induced augmentations in
164 plasma epinephrine, and skeletal muscle *Pgc-1α* expression. As the PVH and AH are located in
165 close proximity to each other (the AH is located at ventral side of the PVH), thus the light source
166 can reach to both areas based on the theoretical irradiance value calculation
167 (https://web.stanford.edu/group/dlab/cgi-bin/graph/chart.php), it is possible that the PVH
168 stimulation also affects the AH. Therefore, going forward, we will refer to optogenetic stimulation
169 in this region as the PVH/AH stimulation instead of the PVH stimulation. We inserted the optic
170 fiber probe into each area followed by an injection of AAV-DIO-ChR2 into the VMH of *Sf-1* Cre
171 mice (Figure 4A). Intriguingly, all terminal stimulations of VMHdm/c^{SF-1} neurons significantly
172 increased blood glucose (Figure 4B). While stimulation in each area also increased plasma
173 epinephrine (mean values ± SEM ; 1919 ± 324, 3869 ± 922, 3782 ± 594, 2759 ± 188, 5145 ± 841,
174 and 6311 ± 836 pg/mL for mCherry, aBNST, POA, AH, PVH/AH, and PAG, respectively), the
175 most striking differences were observed after terminal stimulation of VMHdm/c^{SF-1} neurons in the
176 PVH/AH and PAG (Figure 4C). We found that *Pgc-1α* total mRNA expression levels were
177 significantly increased in the terminal stimulation of the POA and PVH/AH (Figure 4D). *Pgc-1α-*
178 *1* mRNA expression levels were significantly increased in the terminal stimulation in the AH and
179 PVH/AH (Figure 4E). *Pgc-1α-2* and *-3* mRNA expression levels were significantly increased in

180 the terminal stimulation in the PVH/AH and PAG (Figure 4G). Finally, *Pgc-1α-4* mRNA
181 expression levels were significantly increased in the terminal stimulation in the PVH/AH. Of note,
182 although the terminal stimulation in the aBNST, POA, and AH did not statistically increase RNA
183 levels of skeletal muscle *Pgc-1α-2, -3,* and *-4*, the mean values were higher than those in the control
184 group. Collectively, we conclude that VMHdm/c^{SF-1} neuronal projections to the PVH/AH and PAG
185 have greater contributions to the regulation of skeletal muscle *Pgc-1α* mRNA expression and
186 plasma epinephrine. However, other projection sites likely contribute as well, indicating that
187 VMHdm/c^{SF-1} neurons use neurocircuits that are functionally redundant to regulate the
188 sympathoadrenal activity.

189 A previous study found that VMHdm/c^{SF-1} neurons project to downstream sites
190 collaterally[23]. For example, VMHdm/c^{SF-1} neurons projecting to the PAG also send axons to the
191 AH[30]. Each VMHdm/c^{SF-1} neuron likely projects to multiple sites, especially to the areas are
192 topographically adjacent, such as aBNST and POA or the AH and PVH. In other words, when the
193 terminal activation of VMHdm/c^{SF-1} neurons at one downstream area occurs, back-propagated
194 neuronal activation could happen in other non-stimulated areas. To determine whether it is the
195 case, we assessed Fos expression after the terminal activation of VMHdm/c^{SF-1} neurons in the
196 aBNST, POA, AH, PVH/AH, and PAG as well as the soma stimulation of VMHdm/c^{SF-1} neurons
197 (Figure 5A and B). We compared the stimulated side (right hemisphere) and the non-stimulated
198 side (left hemisphere). As shown (Figure 1C), the optogenetic stimulation of the soma of
199 VMHdm/c^{SF-1} neurons (Figure 5O and P) significantly increased Fos expression in the stimulated
200 side of the VMH (Figure 5Q). Intriguingly, the soma activation of VMHdm/c^{SF-1} neurons
201 significantly increased Fos expression only in the PVH and AH (Figure 5Q). We did not find distal
202 neuronal propagations by the terminal activation in the POA, PVH/AH, AH, and PAG (Figure 5H,

K, N, Q, and T). The terminal stimulation in the aBNST increased Fos expression in distal site PAG (Figure 5E). However, it is unclear that Fos expression in the PAG was induced by the distal propagation as Fos expression in the VMH was not changed after aBNST stimulation (Figure 5E). We frequently observed Fos-expression in the sites proximal to the stimulated site. For instance, the aBNST stimulation induced Fos-expression in the POA (Figure 5E). Likewise, the AH stimulation induced Fos-expression in the PVH (Figure 5K), and the PVH/AH stimulation induced Fos-expression in the POA and VMH (Figure 5N). Fos expression in the stimulated hemisphere of AH was significantly higher of all the stimulation sites (Figure 5E, H, K, N, Q, and T), suggesting that these Fos-inductions in the AH may be the secondary rather than direct propagated activation. Collectively, Fos expression data indicated that each single VMHdm/c^{SF-1} neuronal axon projects many downstream sites collaterally, strengthening the idea of functionally redundant VMHdm/c^{SF-1} neuronal circuits that regulate the SNS.

Discussion

Here we demonstrate that VMHdm/c^{SF-1} neuronal circuits regulate skeletal muscle *Pgc-1α* mRNA via the sympathoadrenal-released epinephrine coupled with β2AdR. Our data further predict that VMHdm/c^{SF-1} neurons collaterally project multiple presympathetic nodes in the CNS that possess redundant functions to regulate the sympathoadrenal activation. The VMH facilitates glucose uptake in skeletal muscle and brown adipose tissue (BAT) and fatty acid mobilization from white adipose tissues (WAT) by direct sympathetic innervation rather than the sympathoadrenal drive[32-36]. Intriguingly, these studies have demonstrated that direct sympathetic innervation is key for VMH-induced glucose uptake and lipolysis in BAT and skeletal muscle rather than the sympathoadrenal activity[32,33,35,36]. Contrary to these previous findings, results in this study highlight the importance of the sympathoadrenal activity for VMHdm/c^{SF-1} neurons-induced skeletal muscle *Pgc-1α* expression. Because VMH neurons are genetically heterogenous[37,38], it is possible that VMHdm/c^{SF-1} neurons regulate skeletal muscle function primarily via sympathoadrenal activity, while other subtypes of neurons in the VMH mediate skeletal muscle glucose uptake via the direct sympathetic innervation. Optogenetic activation of leptin receptors-expressing neurons in the VMHdm/c does not affect blood glucose, plasma glucagon, and plasma insulin levels[22], supporting the notion that functional segregation may exist within the VMHdm/c neuronal subgroups. Further studies are warranted to reveal the mechanistic differences among the genetically distinctive neuronal groups within the VMHdm/c that regulate skeletal muscle function.

PGC-1α is one of the key molecules regulating a wide range of skeletal muscle physiology[39]. PGC-1α-1 is "classic" PGC-1α, and regulates mitochondrial function, glucose and fat metabolism[14,29]. PGC-1α-4 regulates the protein synthesis[14,29]. The physiological role of PGC-1α-2 and -3 are still not clear. It is predicted that they contribute to angiogenesis, epithelial function,

238 chromosomal maintenance, and cholesterol metabolism[16]. PGC-1α-1 is derived from the proximal
239 promoter region of PGC-1α locus, and PGC-1α-2, -3, and -4 are derived from the distal promoter
240 region[10]. Intriguingly, running wheel activity and treadmill exercise activate the distal promoter
241 region but not the proximal promoter region[18,40]. Furthermore, β2AdR agonist also only initiates
242 the transcription of PGC-1α exclusively at the proximal promoter region[18,40], leading to increased
243 mRNA levels of PGC-1α-2, -3, and -4, but not PGC-1α-1[16]. These data indicate the importance of
244 the CNS→the SNS→skeletal muscle β2AdR axis for the regulation of skeletal muscle PGC-1α in
245 response to exercise. Our data demonstrate that VMHdm/c^{SF-1} neurons can regulate PGC-1α-2, -3,
246 and -4, but not -1, further strengthening the idea that these neurons are important for exercise-
247 induced augmentation of skeletal muscle function.

248 VMHdm/c^{SF-1} neuronal activation increases circulating epinephrine, and ADX completely
249 blocks VMHdm/c^{SF-1} neuronal-induced skeletal muscle *Pgc-1α* expression (Figure 2), suggesting
250 that epinephrine secretion from the adrenal grand is essential for VMHdm/c^{SF-1} neuronal regulation
251 of skeletal muscle function. Because the adrenal gland secretes many endocrine hormones, we
252 must consider the contribution of non-catecholamines hormones to VMHdm/c^{SF-1} neuronal-
253 induced skeletal muscle *Pgc-1α* expression. For instance, optogenetic activation of VMHdm/c^{SF-1}
254 neurons increases blood corticosterone[22]. Thus, it is possible that the surge of corticosterone from
255 the adrenal gland also contributes to VMHdm/c^{SF-1} neuronal-induced skeletal muscle *Pgc-1α*.
256 Corticosterone supplement (Figure 2B) can only provide physiologically stable corticosterone
257 levels but can not imitate endogenous dynamics of corticosterone releases. However,
258 dexamethasone (DEX) treatments suppress PGC-1α in skeletal muscle cell lines[41], and in the testis
259 of *in vivo* mouse model[42]. Glucocorticoid receptors (GRs) are expressed in skeletal muscle, and
260 skeletal muscle-specific GR-KO mice show increased lean mass[43], which is in line with the fact

261 that DEX can induce atrophy[44]. Therefore, we conclude that corticosterone unlikely contributes to
262 the induction of skeletal muscle PGC-1α after VMHdm/c^{SF-1} neuronal activation. However, further
263 studies are necessary to determine that epinephrine is the only factor in the adrenal gland that
264 contributes to VMHdm/c^{SF-1} neuronal-induced skeletal muscle *Pgc-1α*.

265 A large body of literature has concluded that β2AdR signaling is key to the regulation of
266 skeletal muscle PGC-1α expression[31], and ultimately orchestrating protein synthesis/degradation,
267 glucose and fat metabolism, and angiogenesis[9,10,40]. Our study extends these findings to show that
268 the sympathoadrenal activity coupled with β2AdR is essential for VMHdm/c^{SF-1} neuronal-induced
269 skeletal muscle *Pgc-1α* expression (Figure 3). β2AdR is expressed throughout the body[18], and even
270 within the skeletal muscle, β2AdR is expressed in a variety of cell types including skeletal muscle
271 cells, smooth muscle cells (blood vessels), and endothelial cells[31,45]. In addition, recent studies
272 highlight the key role of β2AdR at the neuromuscular junctions (NMJs) to regulate acetylcholine
273 and acetylcholine receptors[46,47]. As we used global β2 AdR KO mice, we can not formally exclude
274 the possibility that β2AdR in the non-skeletal muscle organs are actually essential. Further studies
275 using tissue specific β2AdR manipulation (e.g., deletion of β2AdR in specifically skeletal or
276 smooth muscle cells) are necessary to decipher the precise targets of VMHdm/c^{SF-1} neurons and
277 the sympathoadrenal axis.

278 The terminal activation of VMHdm/c^{SF-1} neurons in the PVH/AH and PAG significantly
279 increases blood epinephrine and skeletal muscle *Pgc-1α-2 and -3* mRNA (Figure 4). Because the
280 PVH and PAG directly project to the sympathoadrenal preganglionic neurons in the
281 intermediolateral nucleus of the spinal cord[48-51], it is predicted that activation of these areas can
282 have more profound effects on the sympathoadrenal activity. By comparing the results of the
283 PVH/AH and AH stimulation (Figure 4), it is likely that VMHdm/c^{SF-1} neurons projecting to the

284 PVH substantially contribute to the regulation of the SNS activity than that to the AH. Because
285 ADX completely diminishes augmented blood glucose by VMHdm/c^{SF-1} neuronal stimulation
286 (Figure 2), epinephrine release by the SNS activation is likely required for the augmented blood
287 glucose levels. Interestingly, the terminal activation in all sites we investigated significantly
288 increased blood glucose (Figure 4). Taken together, blood glucose data (Figure 4) indicate that all
289 sites we investigated can activate the sympathoadrenal activity, although the degree of the
290 sympathoadrenal activation may vary. In fact, the mean value of blood epinephrine, skeletal
291 muscle *Pgc-1* mRNA levels in all the sites are higher than control group (Figure 4), suggesting
292 that all sites we investigated contribute to VMHdm/c^{SF-1}-neuronal regulation of the
293 sympathoadrenal activity at some extent of degree. Collectively, these data suggest that the
294 downstream sites of VMHdm/c^{SF-1} neurons have redundant functions regarding the augmented
295 sympathoadrenal activity.

296 The Fos expression data (Figure 5) indicate that VMHdm/c^{SF-1} neuronal axon projections
297 are collaterals rather than one-to-one projections[52] as terminal stimulations can induce back-
298 propagated activation in the proximal projected sites of VMHdm/c^{SF-1} neuronal (Figure 5). A
299 previous study using the retrograde tracing method supports this notion as they found that most of
300 VMHdm/c^{SF-1} neurons project to the AH also collaterally send the axon to the PAG[23]. The VMH
301 regulate essential physiological function for survival and high-energy demand situations including
302 counterregulatory actions to hypoglycemia[3], defensive behavior[23,30], and exercise[5,53]. These
303 survival functions have to be executed coordinately at the whole-body level. Considering that
304 collateral VMHdm/c^{SF-1} neuronal circuits are functionally redundant, we propose that similar to
305 monoaminergic neurons[54], VMHdm/c^{SF-1} neurons play a "broadcast" role in the regulation of
306 physiological functions at the whole-body level during emergency or high-energy demand

307 situations. Further studies will be necessary to delineate the degree of contributions of each
308 VMHdm/c^{SF-1} neuronal downstream node to the regulation of metabolism.
309

310 **Limitation of this study**

311 As many previous studies have noted, optogenetic stimulation induces firing patterns that
312 are dissimilar to endogenous firing patterns in many neurons[55]. Therefore, we can not exclude the
313 possibility that our data demonstrate the maximum capability of VMHdm/c^{SF-1} neurons on the
314 regulation of skeletal muscle rather physiological roles of VMHdm/c^{SF-1} neurons. We also used a
315 fixed optogenetic configuration throughout the terminal activations, despite the fact that each site
316 we investigated has a different density of VMHdm/c^{SF-1} neuronal axon and terminals[21]. It is
317 virtually possible that different terminal sites require different firing pattern to execute their
318 function properly. Future studies to use fine-tuning configuration are necessary to test this
319 possibility.

320 As we mentioned above, the inherent limitations of the ADX studies have to be considered.
321 Although we supplied the corticosterone to maintain its physiological levels, the surgical removal
322 of the adrenal gland can compromise many physiological functions directly and indirectly. For
323 instance, we observed that the basal levels of skeletal muscle *Pgc-1α* were decreased in ADX mice
324 (56%, 51%, 96%, 95%, and 72% mean reductions in *Pgc-1α total, Pgc-1α-1, Pgc-1α-2, Pgc-1α-3,*
325 *and Pgc-1α-4* respectively compared to sham control, in Figure 2G). To exclude the possibility
326 that ADX affects the sensitivity of adrenergic receptors, we investigated whether β2AdR agonist
327 can induce skeletal muscle *Pgc-1α* in ADX mice. β2AdR agonist significantly induced skeletal
328 muscle *Pgc-1α*, and there were no significant differences between sham and ADX mice (SFigure
329 2). Thus, ADX unlikely affects the sensitivity of adrenergic receptors in skeletal muscle in our

experimental design. Nonetheless, we have to interpret ADX studies with careful consideration, and future experiments using sophisticated techniques (e.g., genetic-ablation of epinephrine only from the adrenal medulla) will be warranted to further confirm the role of epinephrine releases from the adrenal medulla in the regulation of skeletal muscle physiology.

Conclusion

The CNS-skeletal muscle interactions are important to maintain metabolic homeostasis. The skeletal muscle plays a critical role in the regulation of metabolic homeostasis as it substantially contributes to basal energy expenditure and glucose disposal after meal[13,56]. A large body of studies have built the foundation of neuroanatomy regarding metabolic homeostasis[51]. In the last decade, optogenetic tools have revealed detailed functional neurocircuits regulating metabolism including food intake and glucose metabolism[1,57,58]. This study using optogenetics demonstrates that VMHdm/c^{SF-1} neurons regulate skeletal muscle PGC1-α via epinephrine released from the adrenal gland coupled with β2AdR. In addition, our data suggest that VMHdm/c^{SF-1} neuronal circuits regulating the sympathoadrenal activity are functionally redundant, yet varied contributions from each downstream node to the regulation of the SNS likely exist (SFigure 3). Our study advances the understanding of brain-skeletal muscle communications and implies the significant contributions of VMHdm/c^{SF-1} neurons→sympathoadrenal axis to beneficial effects of exercise on skeletal muscle.

349 **Experimental Procedure**

350

351 **Genetically-Engineered Mice**

352 *Sf-1*-Cre mice were obtained from the Jackson Laboratory (US; Catalog# 012462). *Abrb2* KO mice
353 were derived from β-null mice[59], which was kindly provided by Dr. Bradford Lowell (Harvard
354 Medical School). The sequences of genotyping primers are followings; for *Sf-1*-Cre,
355 aggaagcagccctggaac, aggcaaattttggtgtacgg, agaaactgctccgctttcc with expected bands sizes of 627
356 bp for internal control and 236 bp for *Sf-1*-Cre; for *Abrb2* KO, cacgagactagtgagacgtg,
357 accaagaataaggcccgagt, ccgggaatagacaaagacca with expected bands sizes of 225 bp for the wild-
358 type allele and 410 bp for the knockout allele. *Sf-1*-Cre and *Abrb2* KO mice were bred to generate
359 *Sf-1*-Cre::*Abrb2*$^{KO/KO}$ and *Sf-1*-Cre::*Abrb2*$^{WT/WT}$ mice. *Sf-1*-Cre mice were on a C57BL/J6
360 background and other mice are on a mixed background (C57BL/J6 and FVB.129). We used 3-6
361 month-old male mice whose body weights were above approximately 25-30 grams. All mice were
362 fed a normal chow diet. Animal care was according to established NIH guidelines, and all
363 procedures were approved by the Institutional Animal Care and Use Committee of the University
364 of Texas Southwestern Medical Center and University of Texas Health San Antonio.

365

366 **AAV injections and optic fiber probe insertions**

367 Recombinant AAVs were purchased from the Vector Core at the University of North Carolina at
368 Chapel Hill, US. rAAV5-EF1α-DIO-mCherry (3.3 x 10^{12} VM/mL), rAAV5-EF1α-DIO-
369 ChR2(H134R)-mCherry (3.4 x 10^{12} VM/mL), and rAAV5-EF1α-DIO-ChR2(H134R)-EGFP (3.2
370 x 10^{12} VM/mL) were unilaterally administered into the right side of the VMH of mice using a
371 UMP3 UltraMicroPump (WPI, US) with 10 μL NanoFil microsyringe (WPI) and 35G NanoFil

372 beveled needle (WPI; Catalog# NF35BV-2). The volume of AAVs was 1000 nL at the rate 100
373 nL per minute, and the needle was left for another 5 minutes after the injection was finished. The
374 face of beveled needle was placed towards the center of the brain. The coordinates of VMH-
375 microinjection were AP; −1.4 L +0.5, and D −5.5 (from Bregma). The optic fiber probe was
376 inserted as following coordinates; the VMH (AP; −1.4, L +0.5, and D −5.0), aBNST (AP; 0.3, L
377 +0.5, and D −3.75), POA (AP; 0.4, L +0.25, and D −4.5), AH (AP; −0.9, L +0.5, and D −4.75),
378 PVH/AH (AP; −0.8, L +0.25, and D −4.5), and PAG (AP; −4.3, L +0.2, and D −2.0). The
379 configuration of the probe for the VMH stimulation was 400 µm Core, 0.5NA, Ø2.5 mm ceramic
380 ferrule, and 6mm length (RWD Life science Inc, US and Doric Lenses, Canada). The configuration
381 of probe for other sites was 200 µm Core diameter, 0.39NA, Ø2.5 mm Ceramic Ferrule diameter,
382 and with varied length varied (3-5 mm depend on the place) (RWD Life science Inc, US and Doric
383 Lenses, Canada). The fiber probe was secured by adhesion bond (Loctite 454, Loctite Inc, US).
384 Mice were allowed to recover for at least three weeks after the AAV injections to fully express
385 recombinant proteins.
386

387 **Optogenetics**

388 The light emitting diode (LED) driver (Thorlabs, US; DC4104) with fiber-coupled LED (Thorlabs;
389 Catalog# M470F3) was used for the VMH stimulation, and the laser unit (Opto engine LLC, US;
390 Catalog# MDL-III-470) was used for the terminal of VMHdm/c^{SF-1} neuronal stimulations. The
391 power of tips was set to ~1 mW/mm^2 for the VMH stimulation and ~10 mW/mm^2 for the terminal
392 stimulations. The customed transistor-transistor logic generator was built based on the design by
393 the University of Colorado Optogenetics and Neural Engineering Core. Rotary joint patch cable
394 (Thorlabs; Catalog# RJPSF4 for LED and RJPFF4 for the laser) was used to connect either fiber-

395 coupled LED or the laser unit. The quick-release interconnect (Thorlabs; Catalog# ADAF2) was
396 used to connect the rotary joint patch cable to the fiber probe attached to mouse head. The
397 stimulation was set to; 5 ms duration, 20 Hz, 2 seconds activation and 2 seconds rest cycle, 30
398 minutes (Figure 1B).
399

400 **Adrenalectomy**

401 Skin and muscle incisions (approximately 1 cm) were made close to the abdominal area where
402 kidney was located. Both the adrenal glands were removed by tying with sterile suture. The sham
403 operation was performed as same as ADX surgery except for removing the adrenal glands. The
404 corticosterone water (75 µg/mL, vehicle was sterile 1% ethanol/0.9% NaCl water) was provided
405 with ADX mice, and vehicle was provided with sham mice.
406

407 **Immunohistochemistry and Fos counting**

408 Mouse brains were prepared as previously described[60,61]. Anti-cFos (Sigma, US; Catalog# F7799,
409 batch #0000102540) and secondary fluorescent antibodies (Thermofisher Inc, US; Catalog# A-
410 21202 and A-21203, Lot#WF320931 and WD319534, respectively) were used. Dilution rates for
411 antibodies were 1:1000 for first antibody and 1:200 for second antibodies. Images were captured
412 by fluorescence microscopies (Keyence US, US; Model: BZ-X710, Leica Inc, US; Model DM6
413 B). Exposure of captured images was adjusted, and each area (aBNST, POA, AH, PVH, VMH,
414 and PAG) was clipped by Photoshop. Clipped images were exported to Fiji, and the number of
415 cells expressing Fos was counted by particle measurement function (Figure 5B).
416

417 **Assessment of glucose, catecholamines, and hormone levels in the blood**

418 Blood glucose was measured by a glucose meter as previously described[6,61,62]. Plasma
419 catecholamines and hormones levels were measured as previously described[6,61]. Briefly, the
420 plasma catecholamines were analyzed by the Vanderbilt Hormone Assay & Analytical Services
421 Core. Plasma Glucagon (Mercodia Inc, US; Catalog#10-1281-01), insulin (Crystal Chem Inc, US;
422 Catalog# 90080), and corticosterone (Cayman Chemical, US; Catalog #501320) levels were
423 determined by commercially available ELISA kits.
424

425 **Assessment of mRNA**

426 mRNA levels in the TA muscle were determined as previously described[63]. The sequences of the
427 deoxy-oligonucleotides primers are: *Ppargc1a* total (5' tgatgtgaatgacttggatacagaca, and 5'
428 gctcattgttgtactggttggatatg), *Ppargc1a-1* (5' ggacatgtgcagccaagactct, and 5'
429 cacttcaatccacccagaaagct), *Ppargc1a-2* (5' ccaccagaatgagtgacatgga, and 5' gttcagcaagatctgggcaaa),
430 *Ppargc1a-3* (5' aagtgagtaaccggaggcattc, and 5' ttcaggaagatctgggcaaaga), *Ppargc1a-4* (5'
431 tcacaccaaacccacagaaa, and 5' ctggaagatatggcacat), and *18S* (5' catgcagaacccacgacagta and 5'
432 cctcacgcagcttgttgtcta).
433

434 **Data analysis and statistical design**

435 The data are represented as means ± S.E.M. GraphPad PRISM version 9 (GraphPad, US) was used
436 for the statistical analyses and $P<0.05$ was considered as a statistically significant difference. A
437 detailed analysis was described in Supplemental Table 1. The sample size was decided based on
438 previous publications[6,60-67], and no power analysis was used. Experiments were replicated in
439 Figure 1, 2, 3, and Figure 4B. We did not carry out replicate experiments for data shown in Figure

4C-H and 5. Figures were generated by PRISM version 9, Illustrator 2021, and Photoshop 2021 (Adobe Inc, US).

Acknowledgement

We thank Glenn Toney at UT Health San Antonio (UTHSA) for valuable advice, Nancy Gonzalez and Harun A. Khan (UTHSA) for the technical assistant, Juri C. Fujikawa for providing illustrations, and Steven Wyler, Ryan Reynolds, Luis Leon Mercado, Syann Lee, and Joel. K. Elmquist (UTSW) for valuable comments on the manuscript. This work was supported by the University of Texas System (UT Rising STARs to T.F.), and San Antonio Area Foundation (to T.F.)

Competing interests

The authors do not have any conflict of interests.

Contribution

T.Y. designed, performed and analyzed experiments, and edited the manuscript. S.F., A.H., Z.S., J.L., A.S.T., and A.K.S., performed experiments. T.F. designed, performed, supervised, and analyzed experiments, and wrote and finalized the manuscript.

458 **Figure Legends**

459 **Figure 1. Optogenetic activation of VMHdm/c^{SF-1} neurons increases mRNA levels of skeletal**
460 **muscle *Pgc1-α*** (**A**) Schematic figure of targeting site of VMHdm/c^{SF-1} neurons. (**B**) Experimental
461 design and stimulus setting of optogenetics. (**C**) Representative figures of Fos expression pattern
462 in the hypothalamus of mice expressing ChR2 in SF-1 expression neurons in VMHdm/c
463 (VMHdm/c^{SF-1}::ChR2) after VMHdm/c^{SF-1} neurons stimulation. (**D**) Blood glucose, (**E**) plasma
464 glucagon, (**F**) plasma insulin in mice after VMHdm/c^{SF-1} neuronal stimulation. Control group is
465 composed of mice expressing mCherry in VMHdm/c^{SF-1} neurons (VMHdm/c^{SF-1}::mCherry) (**G**)
466 mRNA expression levels of *Pgc1-α* isoform in skeletal muscle of VMHdm/c^{SF-1}::ChR2 mice after
467 optogenetic stimulation. (**H**) Plasma norepinephrine and (**I**) epinephrine in VMHdm/c^{SF-1}::ChR2
468 mice after optogenetic stimulation. Values are mean ± S.E.M. *** $p < 0.001$, * $p < 0.05$.

469

470 **Figure 2. Adrenalectomy (ADX) completely blocks VMHdm/c^{SF-1} neurons-induced blood**
471 **glucose and skeletal muscle *Pgc1-α* expression** (**A**) Schematic of ADX experimental design. (**B**)
472 Blood corticosterone levels before and after ADX in mice. (**C**) Blood corticosterone levels in ADX
473 mice with and without corticosterone supplementation. (**D**) Representative figures of Fos
474 expression pattern in the hypothalamus of ADX mice expressing ChR2 in SF-1 expression neurons
475 in VMHdm/c (VMHdm/c^{SF-1}::ChR2-ADX) and the number of Fos positive cells in the VMH of
476 VMHdm/c^{SF-1}::ChR2-ADX and sham VMHdm/c^{SF-1}::ChR2 (VMHdm/c^{SF-1}::ChR2-sham). (**E**)
477 Blood glucose, (**F**) plasma glucagon, and (**G**) mRNA expression levels of *Pgc1-α* isoform in
478 skeletal muscle of VMHdm/c^{SF-1}::ChR2-ADX after optogenetic stimulation. Values are mean ±
479 S.E.M. **** $p < 0.0001$, *** $p < 0.001$, ** $p < 0.01$, * $p < 0.05$.

480

481 **Figure 3. Ablation of β2AdR hampers VMHdm/c^{SF-1} neurons-induced skeletal muscle *Pgc1-α*** (**A**) Schematic of experimental design. (**B**) Representative figures of Fos expression pattern in
482
483 the hypothalamus of VMHdm/c^{SF-1}::ChR2 mice lacking β2AdR (VMHdm/c^{SF-1}::ChR2- β2AdR^{KO}),
484 and the number of Fos positive cells in the VMH of VMHdm/c^{SF-1}::ChR2- β2AdR^{KO} and wild-
485 type control (WT) (VMHdm/c^{SF-1}::ChR2-WT). (**C**) Blood glucose and (**D**) plasma glucagon levels
486 in VMHdm/c^{SF-1}::ChR2-β2AdR^{KO} mice after optogenetic stimulation. (**E**) Plasma epinephrine
487 levels in VMHdm/c^{SF-1}::ChR2-β2AdR^{KO} mice with and without optogenetic stimulation. (**F**)
488 mRNA expression levels of *Pgc1-α* isoform in skeletal muscle of ChR2- β2AdR^{KO} mice after
489 optogenetic stimulation. Values are mean ± S.E.M. **** $p < 0.0001$, ** $p < 0.01$, * $p < 0.05$.
490

491 **Figure 4. Downstream nodes of VMHdm/c^{SF-1} neurons are functionally redundant to**
492 **regulate the sympathoadrenal activity**. (**A**) Schematic figure of experimental design. (**B**) Blood
493 glucose levels in VMHdm/c^{SF-1}::ChR2 mice before and after the terminal stimulation of the
494 anterior bed nucleus of the stria terminalis (aBNST), preoptic area (POA), anterior hypothalamus
495 area (AH), paraventricular hypothalamic nucleus (PVH) and AH, and periaqueductal gray (PAG).
496 Control group is VMHdm/c^{SF-1}::mCherry mice after the VMH stimulation. (**C**) Plasma epinephrine
497 levels in VMHdm/c^{SF-1}::ChR2 mice after the terminal stimulation of aBNST, POA, AH, PVH/AH,
498 and PAG. (**D**) mRNA expression levels of *Pgc1-α-Total*, (**E**) *Pgc1-α-1*, (**F**) *Pgc1-α-2*, (**G**) *Pgc1-*
499 *α-3*, and (**H**) *Pgc1-α-4*, skeletal muscle of VMHdm/c^{SF-1}::ChR2 mice after the terminal stimulation
500 of aBNST, POA, AH, PVH/AH, and PAG. Values are mean ± S.E.M. **** $p < 0.0001$, *** $p <$
501 0.001, ** $p < 0.01$, * $p < 0.05$.
502

503 **Figure 5. The terminal activation of VMHdm/c^{SF-1} neurons evokes Fos expression in the**
504 **proximal terminal sites**. (**A**) Schematic figure of experimental design. (**B**) Schematic of Fos
505 expression counts in the nucleus. The brain maps of optic fiber insertion sites of (**C**), aBNST, (**F**)
506 POA (**I**), AH (**L**), PVH/AH, (**O**), VMH, and (**R**) PAG. Representative figures of Fos expression
507 at the terminal sites or soma of VMHdm/c^{SF-1} neurons; (**D**) aBNST, (**G**) POA, (**J**) AH, (**M**)
508 PVH/AH, (**P**), VMHdm/c, and (**S**) PAG. The number of Fos expression cells at the aBNST, POA,
509 AH, PVH/AH, and PAG of VMHdm/c^{SF-1}::ChR2 mice after the terminal stimulation of (**E**)
510 aBNST, (**H**) POA, (**K**) AH, (**N**) PVH/AH, (**Q**) VMHdm/c and (**T**) PAG. Values are mean ± S.E.M.
511 **** $p < 0.0001$, *** $p < 0.001$, ** $p < 0.01$, * $p < 0.05$.
512
513 **Supplemental Figure 1, related to Figure 1.** mRNA expression levels of *Pgc1-α* isoform in
514 skeletal muscle of VMHdm/c^{SF-1}::ChR2 mice exhibiting freeze or burst behavior after optogenetic
515 stimulation. The stimulation configuration was the same as described in Figure 1. Values are mean
516 ± S.E.M., *** $p < 0.001$, * $p < 0.05$.
517
518 **Supplemental Figure 2, related to Figure 2.** mRNA expression levels of *Pgc1-α* isoform in
519 skeletal muscle of ADX mice after β2AdR agonist (clenbuterol 1 mg per kg bodyweight, dissolved
520 in sterile saline solution). Values are mean ± S.E.M. *** $p < 0.001$, ** $p < 0.01$, * $p < 0.05$.
521
522 **Supplemental Figure 3. Summary figure depicting pathways by which VMHdm/c^{SF-1}**
523 **neurons regulate skeletal muscle *Pgc1-α* expression and blood glucose levels via the**
524 **sympathoadrenal gland.**

References

1 Gautron, L., Elmquist, J. K. & Williams, K. W. Neural control of energy balance: translating circuits to therapies. *Cell* **161**, 133-145, doi:10.1016/j.cell.2015.02.023 (2015).

2 Morton, G. J., Meek, T. H. & Schwartz, M. W. Neurobiology of food intake in health and disease. *Nat Rev Neurosci* **15**, 367-378, doi:10.1038/nrn3745 (2014).

3 Stanley, S., Moheet, A. & Seaquist, E. R. Central Mechanisms of Glucose Sensing and Counterregulation in Defense of Hypoglycemia. *Endocr Rev* **40**, 768-788, doi:10.1210/er.2018-00226 (2019).

4 Zhang, Z., Boelen, A., Kalsbeek, A. & Fliers, E. TRH Neurons and Thyroid Hormone Coordinate the Hypothalamic Response to Cold. *Eur Thyroid J* **7**, 279-288, doi:10.1159/000493976 (2018).

5 Fujikawa, T., Castorena, C. M., Lee, S. & Elmquist, J. K. The hypothalamic regulation of metabolic adaptations to exercise. *J Neuroendocrinol* **29**, doi:10.1111/jne.12533 (2017).

6 Fujikawa, T. *et al.* SF-1 expression in the hypothalamus is required for beneficial metabolic effects of exercise. *Elife* **5**, doi:10.7554/eLife.18206 (2016).

7 Zhao, L. *et al.* Steroidogenic factor 1 (SF1) is essential for pituitary gonadotrope function. *Development* **128**, 147-154 (2001).

8 Parker, K. L. *et al.* Steroidogenic factor 1: an essential mediator of endocrine development. *Recent Prog Horm Res* **57**, 19-36 (2002).

9 Handschin, C. & Spiegelman, B. M. The role of exercise and PGC1alpha in inflammation and chronic disease. *Nature* **454**, 463-469, doi:10.1038/nature07206 (2008).

10 Ruas, J. L. *et al.* A PGC-1alpha isoform induced by resistance training regulates skeletal muscle hypertrophy. *Cell* **151**, 1319-1331, doi:10.1016/j.cell.2012.10.050 (2012).

11 Handschin, C. *et al.* Abnormal glucose homeostasis in skeletal muscle-specific PGC-1alpha knockout mice reveals skeletal muscle-pancreatic beta cell crosstalk. *J Clin Invest* **117**, 3463-3474, doi:10.1172/JCI31785 (2007).

12 Benton, C. R. *et al.* Modest PGC-1alpha overexpression in muscle in vivo is sufficient to increase insulin sensitivity and palmitate oxidation in subsarcolemmal, not intermyofibrillar, mitochondria. *J Biol Chem* **283**, 4228-4240, doi:10.1074/jbc.M704332200 (2008).

13 Hawley, J. A., Hargreaves, M., Joyner, M. J. & Zierath, J. R. Integrative biology of exercise. *Cell* **159**, 738-749, doi:10.1016/j.cell.2014.10.029 (2014).

14 Kang, C. & Li Ji, L. Role of PGC-1alpha signaling in skeletal muscle health and disease. *Ann N Y Acad Sci* **1271**, 110-117, doi:10.1111/j.1749-6632.2012.06738.x (2012).

15 Barres, R. *et al.* Acute exercise remodels promoter methylation in human skeletal muscle. *Cell Metab* **15**, 405-411, doi:10.1016/j.cmet.2012.01.001 (2012).

16 Martinez-Redondo, V. *et al.* Peroxisome Proliferator-activated Receptor gamma Coactivator-1 alpha Isoforms Selectively Regulate Multiple Splicing Events on Target Genes. *J Biol Chem* **291**, 15169-15184, doi:10.1074/jbc.M115.705822 (2016).

17 Miura, S. *et al.* An increase in murine skeletal muscle peroxisome proliferator-activated receptor-gamma coactivator-1alpha (PGC-1alpha) mRNA in response to exercise is mediated by beta-adrenergic receptor activation. *Endocrinology* **148**, 3441-3448, doi:10.1210/en.2006-1646 (2007).

18 Miura, S., Kai, Y., Kamei, Y. & Ezaki, O. Isoform-specific increases in murine skeletal muscle peroxisome proliferator-activated receptor-gamma coactivator-1alpha (PGC-

1alpha) mRNA in response to beta2-adrenergic receptor activation and exercise. *Endocrinology* **149**, 4527-4533, doi:10.1210/en.2008-0466 (2008).

19 Uyama, N., Geerts, A. & Reynaert, H. Neural connections between the hypothalamus and the liver. *Anat Rec A Discov Mol Cell Evol Biol* **280**, 808-820 (2004).

20 Shimazu, T. & Minokoshi, Y. Systemic Glucoregulation by Glucose-Sensing Neurons in the Ventromedial Hypothalamic Nucleus (VMH). *J Endocr Soc* **1**, 449-459, doi:10.1210/js.2016-1104 (2017).

21 Lindberg, D., Chen, P. & Li, C. Conditional viral tracing reveals that steroidogenic factor 1-positive neurons of the dorsomedial subdivision of the ventromedial hypothalamus project to autonomic centers of the hypothalamus and hindbrain. *J Comp Neurol* **521**, 3167-3190, doi:10.1002/cne.23338 (2013).

22 Meek, T. H. *et al.* Functional identification of a neurocircuit regulating blood glucose. *Proc Natl Acad Sci U S A*, doi:10.1073/pnas.1521160113 (2016).

23 Wang, L., Chen, I. Z. & Lin, D. Collateral pathways from the ventromedial hypothalamus mediate defensive behaviors. *Neuron* **85**, 1344-1358, doi:10.1016/j.neuron.2014.12.025 (2015).

24 Zhang, J., Chen, D., Sweeney, P. & Yang, Y. An excitatory ventromedial hypothalamus to paraventricular thalamus circuit that suppresses food intake. *Nat Commun* **11**, 6326, doi:10.1038/s41467-020-20093-4 (2020).

25 Berndt, A. *et al.* High-efficiency channelrhodopsins for fast neuronal stimulation at low light levels. *Proc Natl Acad Sci U S A* **108**, 7595-7600, doi:10.1073/pnas.1017210108 (2011).

26 Dhillon, H. *et al.* Leptin directly activates SF1 neurons in the VMH, and this action by leptin is required for normal body-weight homeostasis. *Neuron* **49**, 191-203 (2006).

27 Shimazu, T., Fukuda, A. & Ban, T. Reciprocal influences of the ventromedial and lateral hypothalamic nuclei on blood glucose level and liver glycogen content. *Nature* **210**, 1178-1179 (1966).

28 Flak, J. N. *et al.* Ventromedial hypothalamic nucleus neuronal subset regulates blood glucose independently of insulin. *J Clin Invest* **130**, 2943-2952, doi:10.1172/JCI134135 (2020).

29 Martinez-Redondo, V., Pettersson, A. T. & Ruas, J. L. The hitchhiker's guide to PGC-1alpha isoform structure and biological functions. *Diabetologia* **58**, 1969-1977, doi:10.1007/s00125-015-3671-z (2015).

30 Kunwar, P. S. *et al.* Ventromedial hypothalamic neurons control a defensive emotion state. *Elife* **4**, doi:10.7554/eLife.06633 (2015).

31 Lynch, G. S. & Ryall, J. G. Role of beta-adrenoceptor signaling in skeletal muscle: implications for muscle wasting and disease. *Physiol Rev* **88**, 729-767, doi:10.1152/physrev.00028.2007 (2008).

32 Takahashi, A. & Shimazu, T. Hypothalamic regulation of lipid metabolism in the rat: effect of hypothalamic stimulation on lipolysis. *Journal of the autonomic nervous system* **4**, 195-205 (1981).

33 Minokoshi, Y., Saito, M. & Shimazu, T. Sympathetic denervation impairs responses of brown adipose tissue to VMH stimulation. *Am J Physiol* **251**, R1005-1008 (1986).

34 Sudo, M., Minokoshi, Y. & Shimazu, T. Ventromedial hypothalamic stimulation enhances peripheral glucose uptake in anesthetized rats. *The American journal of physiology* **261**, E298-303 (1991).

35 Haque, M. S. *et al.* Role of the sympathetic nervous system and insulin in enhancing glucose uptake in peripheral tissues after intrahypothalamic injection of leptin in rats. *Diabetes* **48**, 1706-1712 (1999).

36 Minokoshi, Y., Haque, M. S. & Shimazu, T. Microinjection of leptin into the ventromedial hypothalamus increases glucose uptake in peripheral tissues in rats. *Diabetes* **48**, 287-291 (1999).

37 Affinati, A. H. *et al.* Cross-species analysis defines the conservation of anatomically segregated VMH neuron populations. *Elife* **10**, doi:10.7554/eLife.69065 (2021).

38 van Veen, J. E. *et al.* Hypothalamic estrogen receptor alpha establishes a sexually dimorphic regulatory node of energy expenditure. *Nat Metab* **2**, 351-363, doi:10.1038/s42255-020-0189-6 (2020).

39 Lira, V. A., Benton, C. R., Yan, Z. & Bonen, A. PGC-1alpha regulation by exercise training and its influences on muscle function and insulin sensitivity. *Am J Physiol Endocrinol Metab* **299**, E145-161, doi:10.1152/ajpendo.00755.2009 (2010).

40 Chinsomboon, J. *et al.* The transcriptional coactivator PGC-1alpha mediates exercise-induced angiogenesis in skeletal muscle. *Proc Natl Acad Sci U S A* **106**, 21401-21406, doi:10.1073/pnas.0909131106 (2009).

41 Rahnert, J. A., Zheng, B., Hudson, M. B., Woodworth-Hobbs, M. E. & Price, S. R. Glucocorticoids Alter CRTC-CREB Signaling in Muscle Cells: Impact on PGC-1alpha Expression and Atrophy Markers. *PLoS One* **11**, e0159181, doi:10.1371/journal.pone.0159181 (2016).

42 Annie, L., Gurusubramanian, G. & Kumar Roy, V. Dexamethasone mediated downregulation of PGC-1alpha and visfatin regulates testosterone synthesis and antioxidant system in mouse testis. *Acta Histochem* **121**, 182-188, doi:10.1016/j.acthis.2018.12.004 (2019).

43 Shimizu, N. *et al.* A muscle-liver-fat signalling axis is essential for central control of adaptive adipose remodelling. *Nat Commun* **6**, 6693, doi:10.1038/ncomms7693 (2015).

44 Pereira, R. M. & Freire de Carvalho, J. Glucocorticoid-induced myopathy. *Joint Bone Spine* **78**, 41-44, doi:10.1016/j.jbspin.2010.02.025 (2011).

45 Conti, V. *et al.* Adrenoreceptors and nitric oxide in the cardiovascular system. *Front Physiol* **4**, 321, doi:10.3389/fphys.2013.00321 (2013).

46 Khan, M. M. *et al.* Sympathetic innervation controls homeostasis of neuromuscular junctions in health and disease. *Proc Natl Acad Sci U S A* **113**, 746-750, doi:10.1073/pnas.1524272113 (2016).

47 Rodrigues, A. C. Z. *et al.* The sympathetic nervous system regulates skeletal muscle motor innervation and acetylcholine receptor stability. *Acta Physiol (Oxf)* **225**, e13195, doi:10.1111/apha.13195 (2019).

48 Strack, A. M., Sawyer, W. B., Platt, K. B. & Loewy, A. D. CNS cell groups regulating the sympathetic outflow to adrenal gland as revealed by transneuronal cell body labeling with pseudorabies virus. *Brain Res* **491**, 274-296, doi:10.1016/0006-8993(89)90063-2 (1989).

49 Jansen, A. S., Nguyen, X. V., Karpitskiy, V., Mettenleiter, T. C. & Loewy, A. D. Central command neurons of the sympathetic nervous system: basis of the fight-or-flight response. *Science* **270**, 644-646, doi:10.1126/science.270.5236.644 (1995).

50 Saper, C. B., Loewy, A. D., Swanson, L. W. & Cowan, W. M. Direct hypothalamo-autonomic connections. *Brain Res* **117**, 305-312, doi:10.1016/0006-8993(76)90738-1 (1976).

51 Saper, C. B. & Stornetta, R. L. The Rat Nervous System, 4th Edition, Chapter 23. *Academic Press*, 629-673, doi:https://doi.org/10.1016/C2009-0-02419-2 (2015).
52 Betley, J. N., Cao, Z. F., Ritola, K. D. & Sternson, S. M. Parallel, redundant circuit organization for homeostatic control of feeding behavior. *Cell* **155**, 1337-1350, doi:10.1016/j.cell.2013.11.002 (2013).
53 Cavalcanti-de-Albuquerque, J. P. & Donato, J., Jr. Rolling out physical exercise and energy homeostasis: Focus on hypothalamic circuitries. *Front Neuroendocrinol* **63**, 100944, doi:10.1016/j.yfrne.2021.100944 (2021).
54 Scammell, T. E., Arrigoni, E. & Lipton, J. O. Neural Circuitry of Wakefulness and Sleep. *Neuron* **93**, 747-765, doi:10.1016/j.neuron.2017.01.014 (2017).
55 Guru, A., Post, R. J., Ho, Y. Y. & Warden, M. R. Making Sense of Optogenetics. *Int J Neuropsychopharmacol* **18**, pyv079, doi:10.1093/ijnp/pyv079 (2015).
56 Egan, B. & Zierath, J. R. Exercise metabolism and the molecular regulation of skeletal muscle adaptation. *Cell Metab* **17**, 162-184, doi:10.1016/j.cmet.2012.12.012 (2013).
57 Sternson, S. M., Atasoy, D., Betley, J. N., Henry, F. E. & Xu, S. An Emerging Technology Framework for the Neurobiology of Appetite. *Cell Metab* **23**, 234-253, doi:10.1016/j.cmet.2015.12.002 (2016).
58 Zimmerman, C. A. & Knight, Z. A. Layers of signals that regulate appetite. *Curr Opin Neurobiol* **64**, 79-88, doi:10.1016/j.conb.2020.03.007 (2020).
59 Bachman, E. S. *et al.* betaAR signaling required for diet-induced thermogenesis and obesity resistance. *Science* **297**, 843-845, doi:10.1126/science.1073160 (2002).
60 Fujikawa, T. *et al.* Leptin engages a hypothalamic neurocircuitry to permit survival in the absence of insulin. *Cell Metab* **18**, 431-444, doi:10.1016/j.cmet.2013.08.004 (2013).
61 Singha, A. *et al.* Leptin Receptors in RIP-Cre(25Mgn) Neurons Mediate Anti-dyslipidemia Effects of Leptin in Insulin-Deficient Mice. *Front Endocrinol (Lausanne)* **11**, 588447, doi:10.3389/fendo.2020.588447 (2020).
62 Singha, A. K. *et al.* Glucose-Lowering by Leptin in the Absence of Insulin Does Not Fully Rely on the Central Melanocortin System in Male Mice. *Endocrinology* **160**, 651-663, doi:10.1210/en.2018-00907 (2019).
63 Fujikawa, T., Chuang, J. C., Sakata, I., Ramadori, G. & Coppari, R. Leptin therapy improves insulin-deficient type 1 diabetes by CNS-dependent mechanisms in mice. *Proc Natl Acad Sci U S A* **107**, 17391-17396, doi:10.1073/pnas.1008025107 (2010).
64 Miyaki, T. *et al.* Noradrenergic projections to the ventromedial hypothalamus regulate fat metabolism during endurance exercise. *Neuroscience* **190**, 239-250, doi:10.1016/j.neuroscience.2011.05.051 (2011).
65 Asterholm, I. W. *et al.* Elevated resistin levels induce central leptin resistance and increased atherosclerotic progression in mice. *Diabetologia* **57**, 1209-1218, doi:10.1007/s00125-014-3210-3 (2014).
66 Williams, K. W. *et al.* Xbp1s in Pomc Neurons Connects ER Stress with Energy Balance and Glucose Homeostasis. *Cell Metab* **20**, 471-482, doi:10.1016/j.cmet.2014.06.002 (2014).
67 Castorena, C. M. *et al.* CB1Rs in VMH neurons regulate glucose homeostasis but not body weight. *Am J Physiol Endocrinol Metab* **321**, E146-E155, doi:10.1152/ajpendo.00044.2021 (2021).

Figure 1

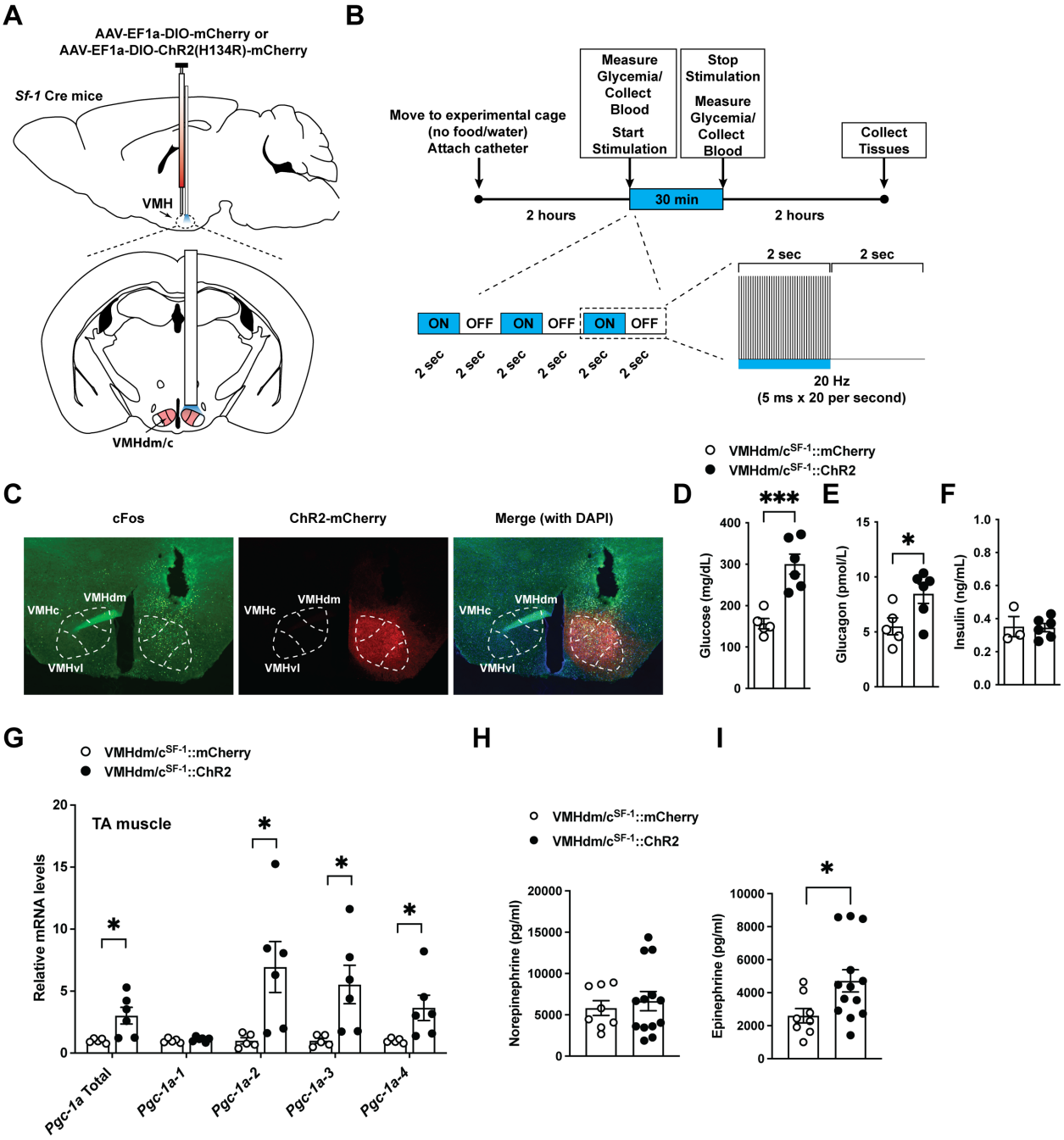
A
AAV-EF1a-DIO-mCherry or
AAV-EF1a-DIO-ChR2(H134R)-mCherry
Sf-1 Cre mice
VMH
VMHdm/c
B
Move to experimental cage
(no food/water)
Attach catheter
Measure
Glycemia/
Collect
Blood
Start
Stimulation
Stop
Stimulation
Measure
Glycemia/
Collect
Blood
Collect
Tissues
2 hours
30 min
2 hours
ON
OFF
ON
OFF
ON
OFF
2 sec
2 sec
2 sec
2 sec
2 sec
2 sec
2 sec
2 sec
20 Hz
(5 ms x 20 per second)
VMHdm/c^SF-1::mCherry
VMHdm/c^SF-1::ChR2
C
cFos
ChR2-mCherry
Merge (with DAPI)
VMHc
VMHdm
VMHvl
D
Glucose (mg/dL)
E
Glucagon (pmol/L)
F
Insulin (ng/mL)
G
TA muscle
Relative mRNA levels
Pgc-1a Total
Pgc-1a-1
Pgc-1a-2
Pgc-1a-3
Pgc-1a-4
H
Norepinephrine (pg/ml)
I
Epinephrine (pg/ml)

Figure 2

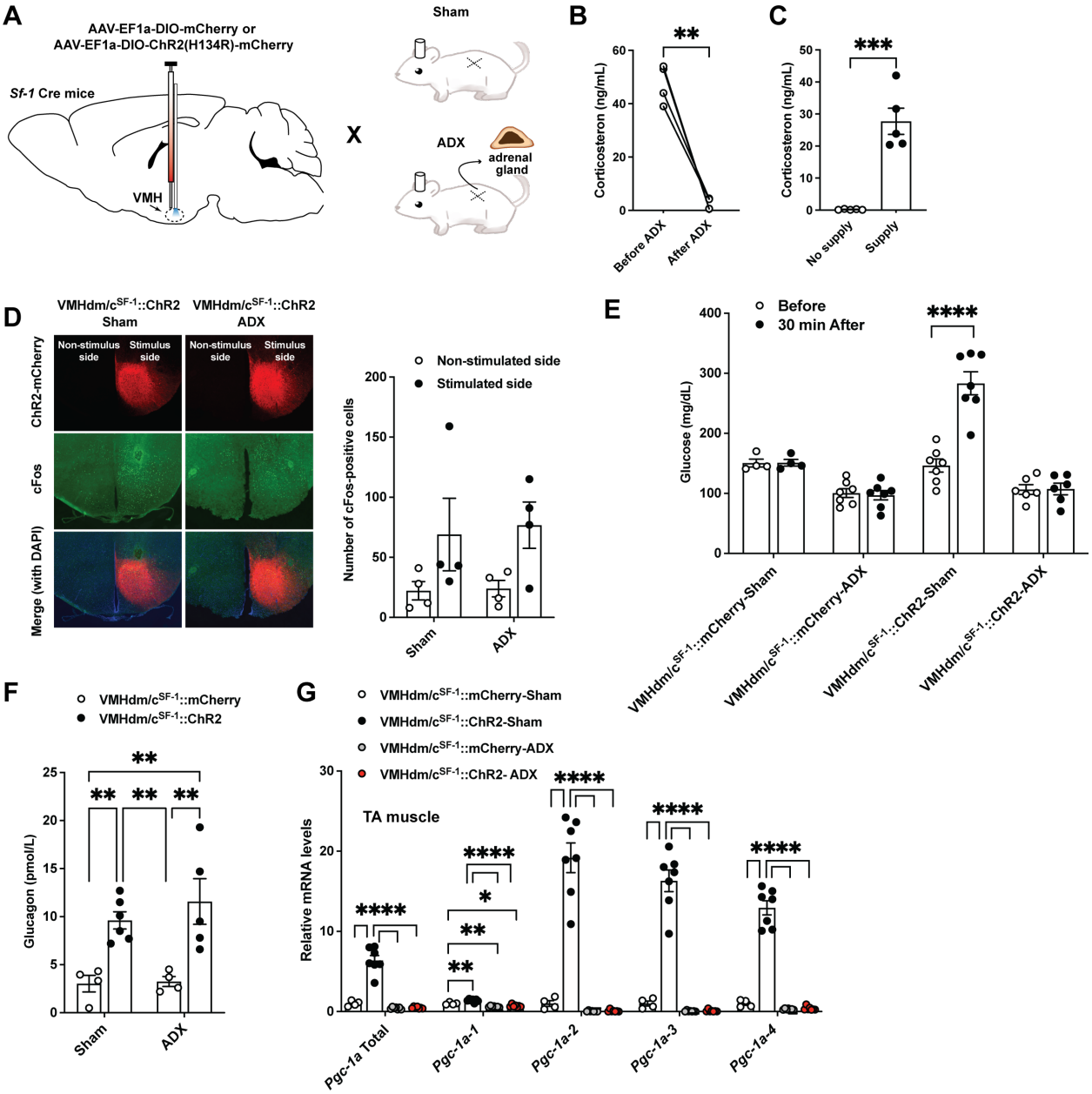
A
AAV-EF1a-DIO-mCherry or
AAV-EF1a-DIO-ChR2(H134R)-mCherry
Sf-1 Cre mice
VMH
X
Sham
ADX
adrenal gland
B
Corticosteron (ng/mL)
Before ADX
After ADX
C
Corticosteron (ng/mL)
No supply
Supply
D
VMHdm/cSF-1::ChR2 Sham
VMHdm/cSF-1::ChR2 ADX
Non-stimulus side
Stimulus side
ChR2-mCherry
cFos
Merge (with DAPI)
Non-stimulated side
Stimulated side
Number of cFos-positive cells
Sham
ADX
E
Before
30 min After
Glucose (mg/dL)
VMHdm/cSF-1::mCherry-Sham
VMHdm/cSF-1::mCherry-ADX
VMHdm/cSF-1::ChR2-Sham
VMHdm/cSF-1::ChR2-ADX
F
VMHdm/cSF-1::mCherry
VMHdm/cSF-1::ChR2
Glucagon (pmol/L)
Sham
ADX
G
VMHdm/cSF-1::mCherry-Sham
VMHdm/cSF-1::ChR2-Sham
VMHdm/cSF-1::mCherry-ADX
VMHdm/cSF-1::ChR2- ADX
TA muscle
Relative mRNA levels
Pgc-1a Total
Pgc-1a-1
Pgc-1a-2
Pgc-1a-3
Pgc-1a-4

Figure 3

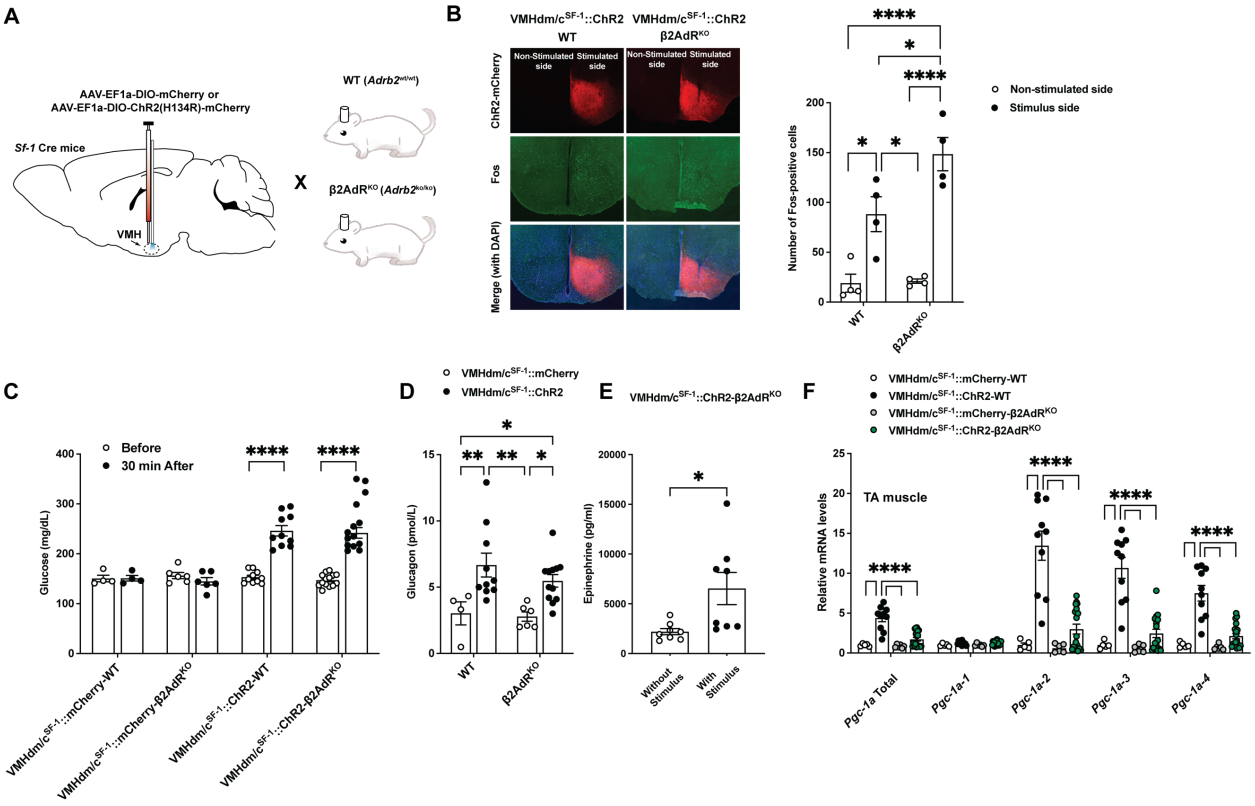
A
AAV-EF1a-DIO-mCherry or
AAV-EF1a-DIO-ChR2(H134R)-mCherry
Sf-1 Cre mice
VMH
X
WT (Adrb2wt/wt)
β2AdRKO (Adrb2ko/ko)
B
VMHdm/cSF-1::ChR2 WT
VMHdm/cSF-1::ChR2 β2AdRKO
Non-Stimulated side
Stimulated side
ChR2-mCherry
Fos
Merge (with DAPI)
Number of Fos-positive cells
Non-stimulated side
Stimulus side
WT
β2AdRKO
C
Before
30 min After
Glucose (mg/dL)
VMHdm/cSF-1::mCherry-WT
VMHdm/cSF-1::mCherry-β2AdRKO
VMHdm/cSF-1::ChR2-WT
VMHdm/cSF-1::ChR2-β2AdRKO
D
VMHdm/cSF-1::mCherry
VMHdm/cSF-1::ChR2
Glucagon (pmol/L)
WT
β2AdRKO
E
VMHdm/cSF-1::ChR2-β2AdRKO
Epinephrine (pg/ml)
Without Stimulus
With Stimulus
F
VMHdm/cSF-1::mCherry-WT
VMHdm/cSF-1::ChR2-WT
VMHdm/cSF-1::mCherry-β2AdRKO
VMHdm/cSF-1::ChR2-β2AdRKO
TA muscle
Relative mRNA levels
Pgc-1a Total
Pgc-1a-1
Pgc-1a-2
Pgc-1a-3
Pgc-1a-4

Figure 4

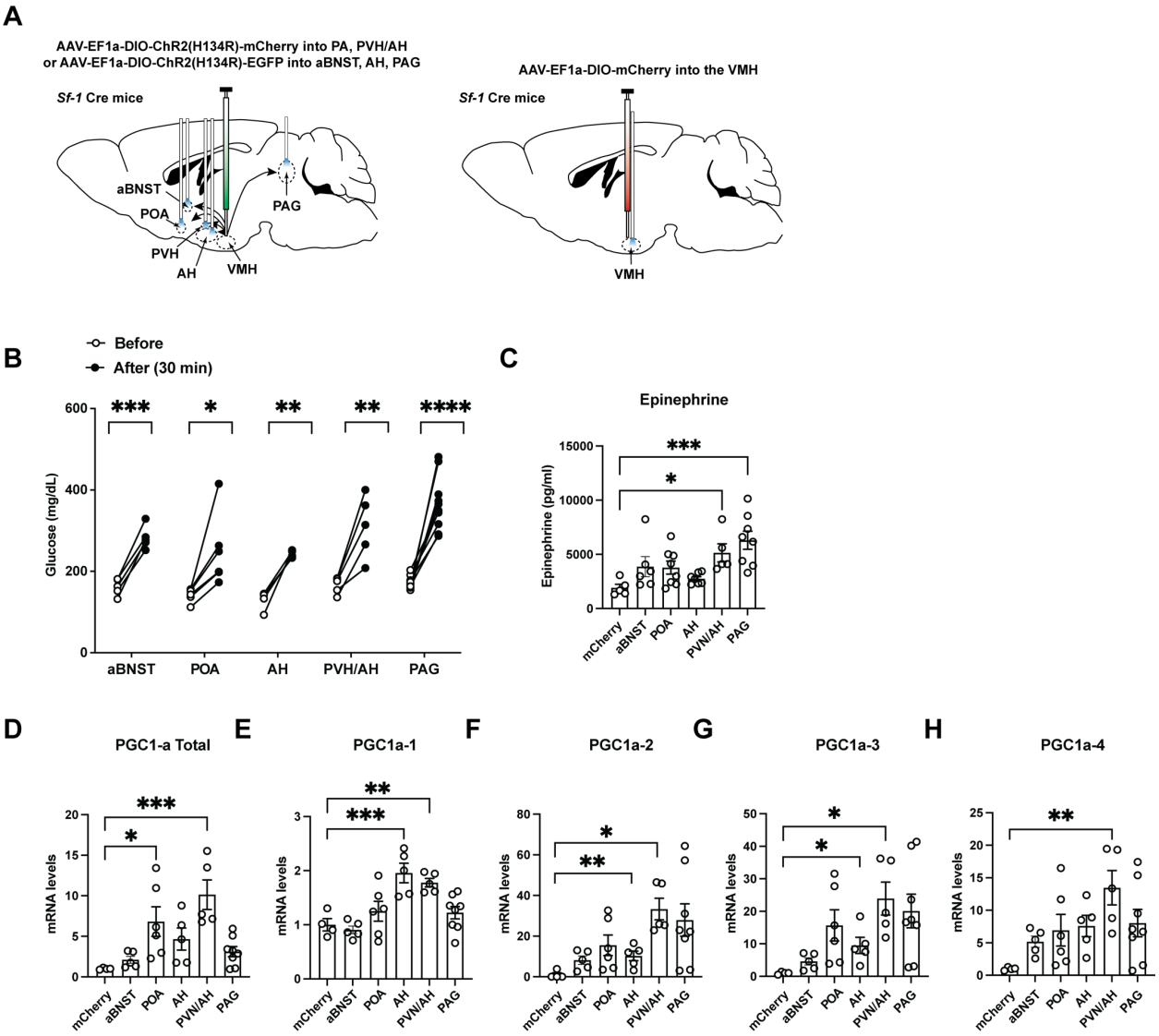
A
AAV-EF1a-DIO-ChR2(H134R)-mCherry into PA, PVH/AH
or AAV-EF1a-DIO-ChR2(H134R)-EGFP into aBNST, AH, PAG
Sf-1 Cre mice
aBNST
POA
PVH
AH
VMH
PAG
AAV-EF1a-DIO-mCherry into the VMH
Sf-1 Cre mice
VMH
B
Before
After (30 min)
Glucose (mg/dL)
aBNST
POA
AH
PVH/AH
PAG
C
Epinephrine
Epinephrine (pg/ml)
mCherry
aBNST
POA
AH
PVN/AH
PAG
D
PGC1-a Total
E
PGC1a-1
F
PGC1a-2
G
PGC1a-3
H
PGC1a-4
mRNA levels

Figure 5

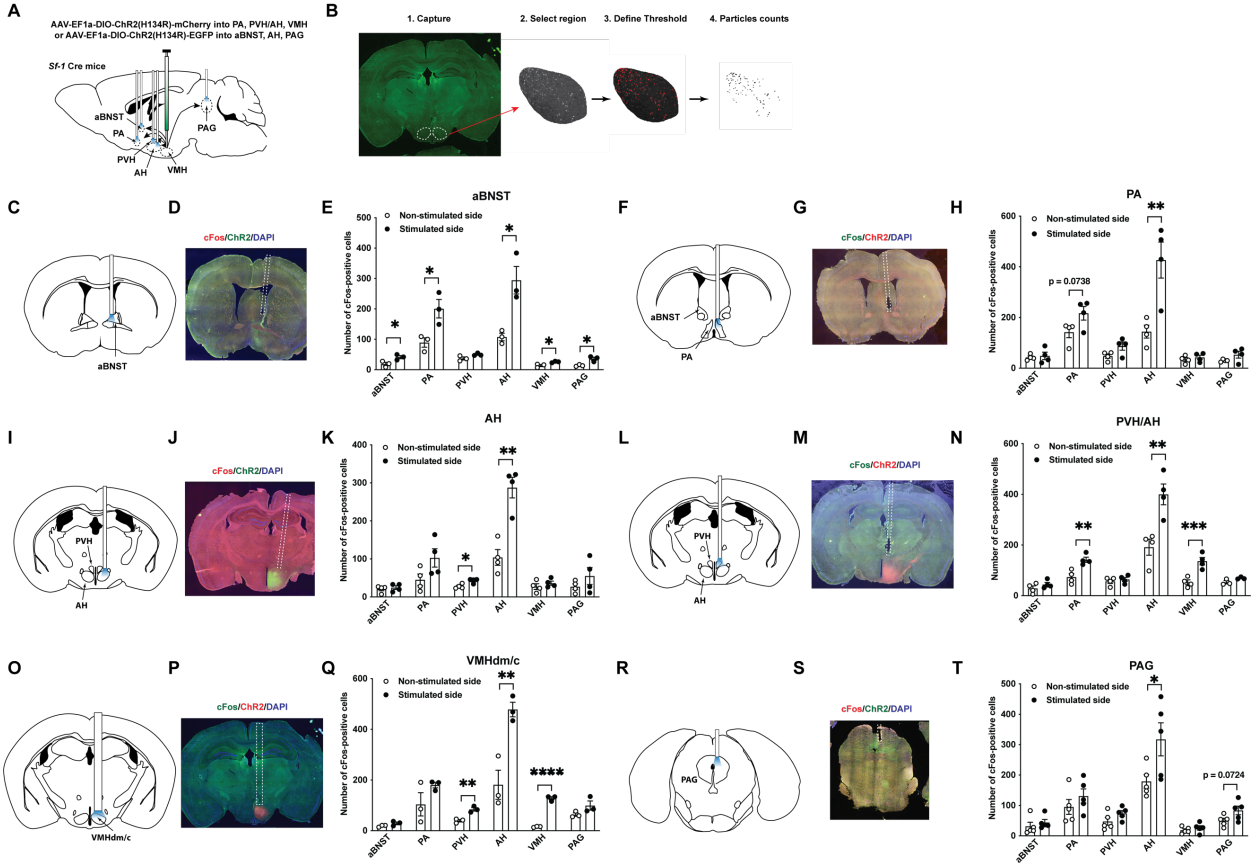
A
AAV-EF1a-DIO-ChR2(H134R)-mCherry into PA, PVH/AH, VMH
or AAV-EF1a-DIO-ChR2(H134R)-EGFP into aBNST, AH, PAG
Sf-1 Cre mice
aBNST
PA
PVH
AH
VMH
PAG
B
1. Capture
2. Select region
3. Define Threshold
4. Particles counts
C
aBNST
D
cFos/ChR2/DAPI
E
aBNST
Non-stimulated side
Stimulated side
Number of cFos-positive cells
F
aBNST
PA
G
cFos/ChR2/DAPI
H
PA
p = 0.0738
I
PVH
AH
J
cFos/ChR2/DAPI
K
AH
L
PVH
AH
M
cFos/ChR2/DAPI
N
PVH/AH
O
VMHdm/c
P
cFos/ChR2/DAPI
Q
VMHdm/c
R
PAG
S
cFos/ChR2/DAPI
T
PAG
p = 0.0724

SFigure 1

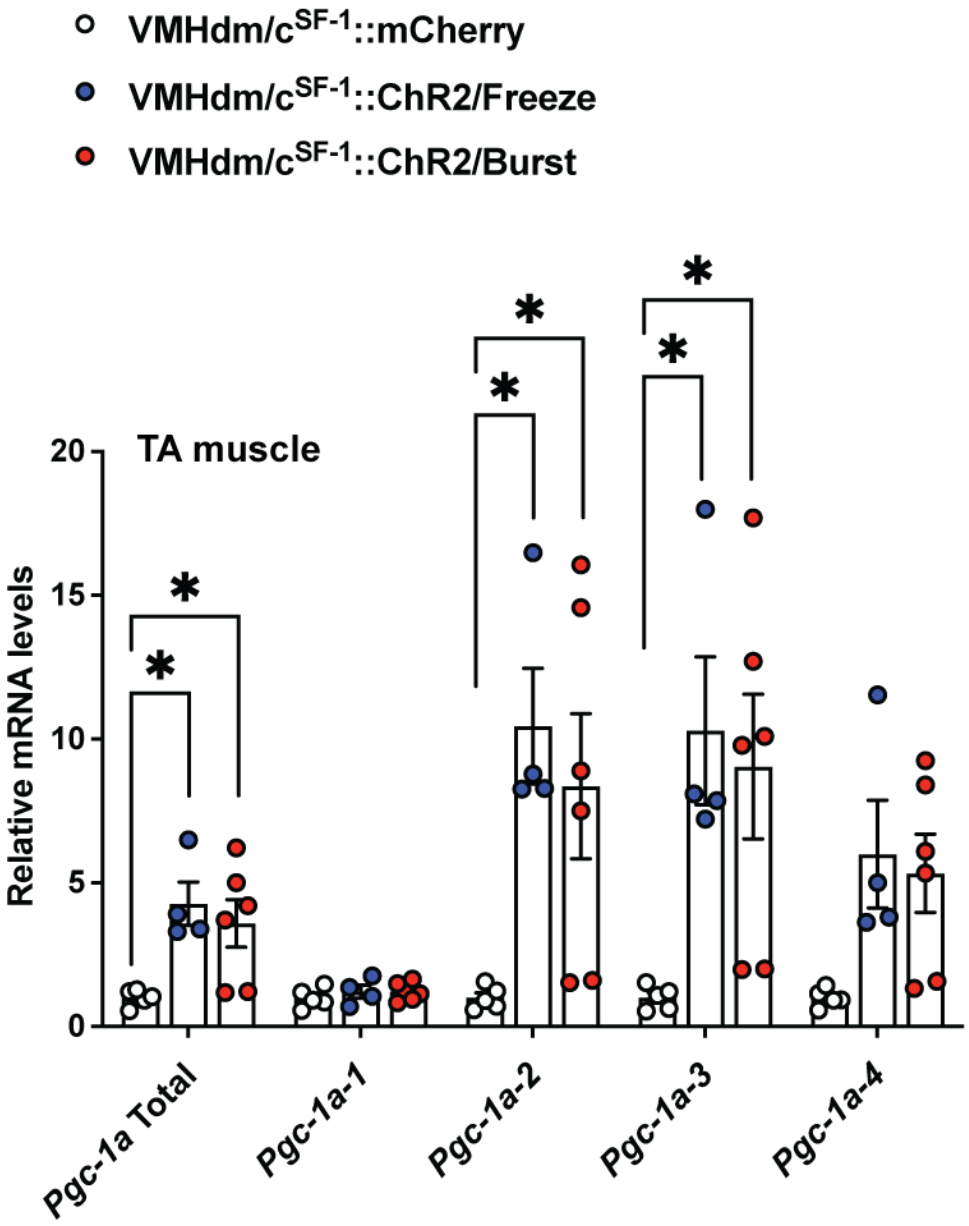
VMHdm/c^{SF-1}::mCherry
VMHdm/c^{SF-1}::ChR2/Freeze
VMHdm/c^{SF-1}::ChR2/Burst
TA muscle
Relative mRNA levels
20
15
10
5
0
*
Pgc-1a Total
Pgc-1a-1
Pgc-1a-2
Pgc-1a-3
Pgc-1a-4

S Figure 2

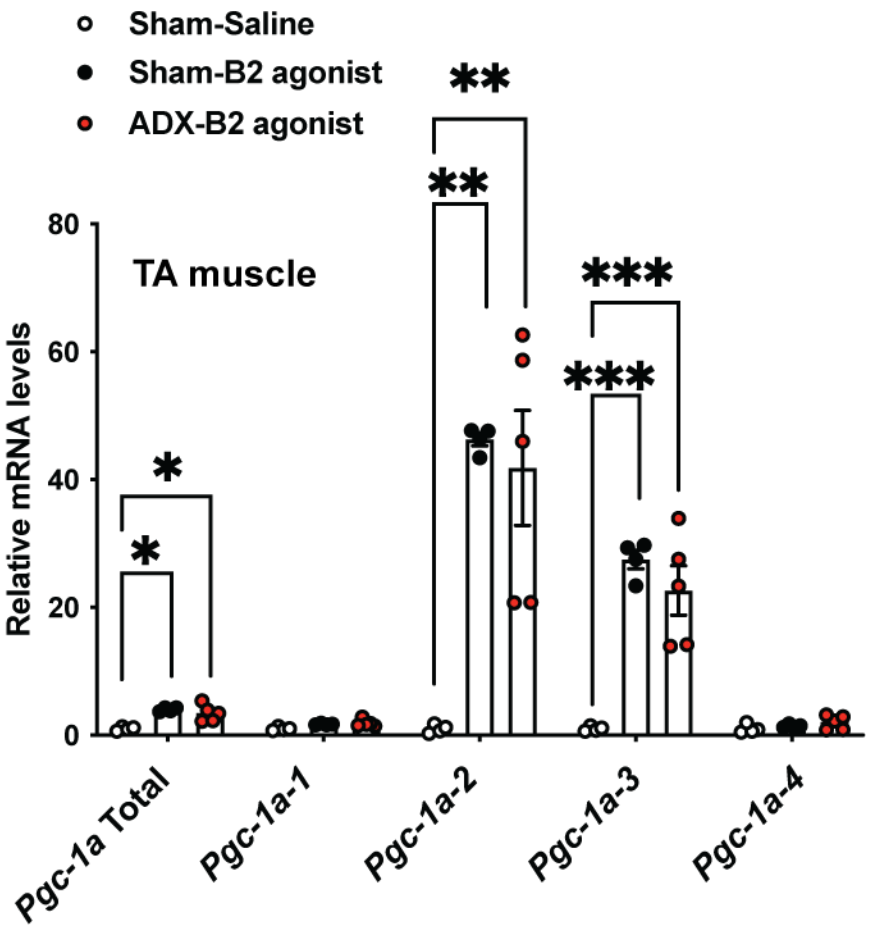
Sham-Saline
Sham-B2 agonist
ADX-B2 agonist
TA muscle
Relative mRNA levels
80
60
40
20
0
*
*
**
**
***
***
Pgc-1a Total
Pgc-1a-1
Pgc-1a-2
Pgc-1a-3
Pgc-1a-4

S Figure 3

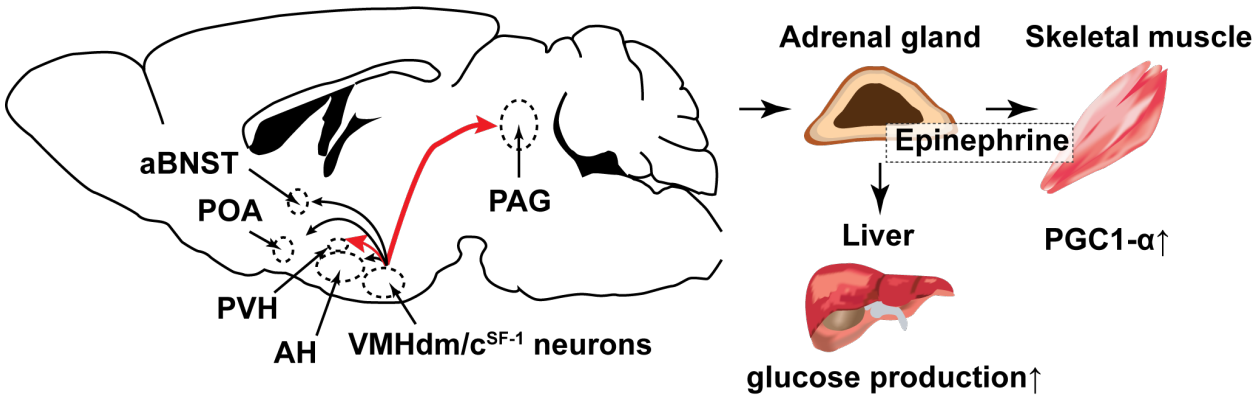
aBNST
POA
PVH
AH
VMHdm/c^{SF-1} neurons
PAG
Adrenal gland
Skeletal muscle
Epinephrine
Liver
PGC1-α↑
glucose production↑